Fillet radius influence for keyway subjected to fatigue: An investigation on an actual application

Mechanical Engineering Science
2025, Vol. XX(X) 1–16

DOI: 10.1177/ToBeAssigned
journals.sagepub.com/home/trr
SAGE

Fillet radius influence for keyway subjected to fatigue: an investigation on an actual application

Matteo Mascolo[1] and Carlo Rosso[1]

Abstract

The keyway is a widely employed solution to link a hub with a shaft. This paper underlines the importance of the fillet radius at the keyway base, highlights the combined effect between bending and torsion and verifies the stress concentration factors present in the literature thanks to Finite Element Method. Starting from a first analytical analysis of the shaft, a series of FE analyses were carried out with the aim of understanding why certain shaft failures occurred. In these analyses, the key presence is considered and the torque is transmitted through it. The analysis reveals that standard verification could fail for some configurations and for the precise evaluation of the fatigue behaviour, for this reason a numerical model is always suggested.

Keywords

Shaft Design, Keyway, Fatigue Life Expectancy, Topological Optimisation, Stress Concentration Factors, Finite Element Analysis

Nomenclature

σ_f^*	Fatigue limit of polished, unnotched test specimen reverse bending [N/mm^2]
μ_s	Static friction coefficient
τ	Shear stress
τ_s	Shear stress due to shear
τ_t	Shear stress due to torsion
σ_b	Normal stress due to bending [N/mm^2]
σ_f	Corrected bending fatigue limit of the shaft [N/mm^2]
σ_u	Ultimate tensile strength [N/mm^2]
τ_m	Mean torsional stress [N/mm^2]
τ_{sy}	Shaft torsional yield stress [N/mm^2]
τ_y	Yield shear stress [N/mm^2]
$^\circ CA$	Shaft crank angle position with respect to the machine volumetric cycle
b	Key width
F_{cr}	Connecting rod force
F_t	Tangential force
h	Key height
I_p	Shaft polar moment of inertia
I_x	Shaft moment of inertia with respect x axis
K_t	Stress concentration factor
l	Key length
M	Bending moment [Nm]
q_A	Distributed reaction force of bearing A
q_B	Distributed reaction force of bearing B
q_{cr}	Connecting rod distributed force
r	Shaft radius
R_A	Reaction force of bearing A
R_B	Reaction force of bearing B

[1] Politecnico di Torino, Department of Mechanical and Aerospace Engineering.

Corresponding author:
Matteo Mascolo, Ph.D Candidate, Department of Mechanical and Aerospace Engineering Politecnico di Torino, Corso Duca degli Abruzzi 24 Torino, Italy
Carlo Rosso, Associate Professor, Department of Mechanical and Aerospace Engineering Politecnico di Torino, Corso Duca degli Abruzzi 24 Torino, Italy
Email: matteo.mascolo@polito.it, carlo.rosso@polito.it

R_θ Shaft rotation constraint

r_{shaft} Fillet radius at keyway base

T Torsional moment [Nm]

Introduction

Even today, keys and keyways remain the simplest solution and, in some cases, the only option to couple a hub and a shaft. The initial studies to define this type of connection date back to the early 20th century. Notably, thanks to Filon (1), the torsional stiffness of various shaft cross sections has been estimated analytically, with a particular focus on the effect of keyways, modelling the cross sections with confocal ellipses and hyperbolas. Several years later, Moore (2) conducted an experimental study to evaluate the impact of keyways on the shaft torsional stiffness. Subsequently Gronwall (3) proposed an analytical model to estimate the stress concentration for a shaft cross section composed of a circle and a circular arc representing the keyway groove. Shepherd (4) extended the model for a shaft with multiple slits under torsion and flexure. Meanwhile Ōkubo (5) introduced a numerical model that combines the effects of fillet radius and the notch's depth over the maximum stress, resulting in a better alignment between the analytical model predictions and experimental data. Following this development of analytical models, several experimental studies were conducted using photo-elastic techniques, which allow the complete definition of the surface stress field (*6*–*15*). Part of these photo-elastic tests have been conducted without the key presence, the keyways in these cases are not directly loaded by the key, consequently, contrary to the majority of applications, this element does not play a role in the torque transmission. Another possibility to study this type of coupling was the electrocoating as reported by Ōkubo et al. (16). In addition to these works where, through different techniques, the stress in the neighbourhood of the keyway groove has been estimated, there are references more inclined to define the fatigue life for a keyed shaft (*17*–*22*). More recent studies (*23*–*25*) suggest a series of keyway topological optimisations, although unfortunately, the majority of the suggested geometries are intrinsically not feasible to realise, representing a hurdle for chip removal processes.

Based on these previous works, this paper resumes the analysis conducted on a non-conventional crank mechanism where several fatigue failures have been identified during its service life. Starting from the analytical estimation of the entire machine working cycle, the nominal stress state is identified and validated by strain gauges experiments. After performing a first shaft verification, following the dimensioning standard ASME (26), the shaft apparently seems to be verified for unlimited. Once recognized that the analytical outcomes do not reflect the stress present in the FE results, a series of investigations have been conducted. Initially, torque and bending superposition were investigated for different fillets at three inspection points. At the same time, the effect of friction has been defined for a standard key coupling. In addition, by varying the ratio between bending and torsion, a stress concentration factor dedicated to bending is defined and estimated for a series of load cases. Last but not least, by taking as a reference a series of papers results and reconstructing the various geometries reported, some literature stress concentration factors have been compared with the ones coming from FE.

Crankshaft Mechanism

The crankshaft considered in this article finds its use in the industrial field on some reciprocating pump models. Different from the standard widely diffused automotive crank mechanism, this type of shaft is composed of multiple bodies linked together by keyways and elastic rings. This solution, compared to a single-body automotive crankshaft, owns some features which make it optimal for low regimes and high torques. Fig. 1 makes evidence of a completely different structure with respect to the internal combustion engine standard: the considered crankshaft is mainly composed of an eccentric and a straight shaft. One of the major benefits of this topological solution is the possibility of using bearings instead of bushings as supporting elements for the shaft and the connecting rod. As previously stated, the crankshaft is characterized by a series of different notches, for each of them the stresses have been estimated, analytically, numerically and through the employment of strain gages. This shaft is supported by two bearings positioned on the minor diameter section: the one positioned near the section variation, identified as bearing A, corresponds to an orientable roller bearing while bearing B, which is a cylindrical roller bearing, is located near the shaft end. To resume, bearing B leaves free the axial movement of the shaft while bearing A locks the shaft's axial and radial movements. The reference coordinate system and the crank mechanism structure are presented in Fig. 1. The material used for the shaft traces the suggestions of CrMo alloy steels present in Shigley (27) textbook, the key is realized in C45 while the eccentric is made in 14NiCr14 carburizing structural steel. The minimum admissible mechanical properties coming from material grades approval, with reference to the material yield strength $R_{p0.2}$ and ultimate tensile strength R_m are reported in Tab. 1.

Crankshaft dimensioning verification to fatigue

Shaft design verification

As a first step to verify the correct shaft sizing, ASME (26) offers a shaft dimensioning standard for power-transmitting shafts. Based on the studies conducted by Gough and Pollard

Table 1. Mechanical properties of the shaft and eccentric.

Component	Material	R_{p02} [MPa]	R_m [MPa]
Shaft	39NiCrMo3	685	880
Eccentric	14NiCr14	635	830
Keyway	C45	430	600

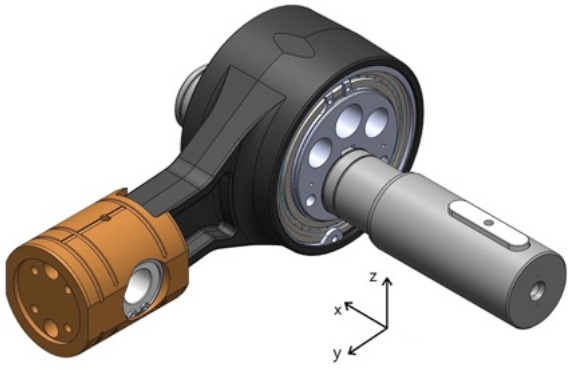

Figure 1. Non-conventional crank mechanism.

(28) and Loewenthal (29), the ASME B106.1M provides an analytical shaft design procedure to define the shaft diameter under combined cyclic bending and torsional load. The method is based on elliptical relation which combines the bending fatigue strength variation with the torque transmitted according to experimental data. The traditional Goodman line provides an acceptable design only in the case where a single kind of stress is acting (i.e. an alternating bending stress superimposed on a steady bending stress) (*18*). For the considered shaft, as for most power-transmitting shafts, a combination of bending and torsional loads are present. To describe their combined effect, according to the distortion energy theory, by following (*18, 19, 29*), the elliptical relation is defined as reported in Eq. 1. As reported in (*30*) and highlighted in Par. Experimental Analysis, the shaft perceives the maximum combined stress during the compression pump phase. Since the force exerted by the piston is constant from about 230 to 360 $^{\circ}CA$, the bending stress is consequently constant too, even if, looking at the shaft with a reference system tied to it, the bending neutral plane and the point of maximum bending stress are rotating. Considering the trend of torsional and bending profile over a complete shaft cycle, that represents the unique load condition for the entire mission of the shaft, it is possible to ascertain their phasing trend since they are a consequence of the same quantity, namely the piston force. This last statement is valid only if it is considered a shaft crank angle and a shaft cross section normal to the x axis, but for a precise location on the shaft surface like the keyway, this claim is no longer true. So, keeping the aforementioned, for the application of this shaft sizing method, it was decided to consider the maximum value of bending and torsion acting on the shaft. This choice surely makes the method's results more conservative.

$$(\sigma_b/{\sigma_f}^*)^2 + (\tau_{\mathbf{m}}/\tau_y)^2 = 1 \tag{1}$$

In the elliptical relation, σ_f^* represents the reversed-bending fatigue limit of the test specimen under bending only, whereas τ_y the torsional yield strength. It's possible to consider the mean stress effect by adopting the Eq. 2 present in (*18*).

$$\sigma_{f,m}^* = \sigma_f^* \left[\left[1 - 77.8 \left(\frac{T_m}{d^3 \sigma_y} \right)^2 \right]^{1/2} - 10.2 \left(\frac{M_m}{d^3 \sigma_u} \right) \right] \tag{2}$$

By rearranging Eq. 1 as reported in (*26*), it is possible to express a first shaft diameter dimensioning as a function of the bending and torsional moments for unlimited life.

$$d = \left[\frac{32SF}{\pi} \sqrt{\left(\frac{M_b}{\sigma_f} \right)^2 + \frac{3}{4} \left(\frac{T_m}{\tau_y} \right)^2} \right]^{1/3} \tag{3}$$

In the general case where both bending and torsional moments acting on the shaft are oscillating, according to (*18*), the shaft diameter can be estimated as:

$$d = \left[\frac{32SF}{\pi} \sqrt{\left(\frac{M_m}{\sigma_u} + \frac{M_a}{\sigma_f} \right)^2 + \frac{3}{4} \left(\frac{T_m}{\tau_y} + \frac{T_a}{\tau_{sy}} \right)^2} \right]^{1/3} \tag{4}$$

Both formulations 3 and 4 request the shaft fatigue limit in case of bending and torsion. Thanks to a series of service factors reported in Tab. 2, either the shaft reverse bending strength σ_f and the shaft torsional yield strength* τ_{sy} have been estimated from the uncorrected test specimen's bending endurance limit σ_f^*. Thus, thanks to the fatigue coefficients k, by means of Eq. 7 and 8, the fatigue bending strength σ_f and the fatigue torsional strength of the shaft τ_{sy} are obtained. The values of fatigue stress concentration factors k_f for bending and torsion have been estimated through Eq. 5 and 6, considering the K_t values reported in (*13, 16, 21*). The microstructural coefficient A is defined according to the shaft material ultimate tensile strength R_m, in accordance with (*22*).

$$q = \frac{1}{A/\sqrt{r}} \tag{5}$$

$$k_f = \frac{1}{K_f} = \frac{1}{1 - q(K_t - 1)} \tag{6}$$

*τ_{xy} also known as σ_{xy} in the anglo-saxon nomenclature

Table 2. Shaft Service Factor.

Factor	Value	Considered Factor
k_a	0.95	Surface F.
k_b	0.78	Size F.
k_c	0.81	Reliability F.
k_d	1.00	Temperature F.
k_e	1.00	Duty F.
Stress C. Factor	Bending	Torsion
$K_{t,0.25}$	4.8	4.8
$K_{t,0.50}$	3.5	4.0
$K_{t,1.00}$	2.6	3.5
Fatigue Factor	Bending	Torsion
$k_{f,0.25}$	0.288	0.288
$k_{f,0.50}$	0.356	0.315
$k_{f,1.00}$	0.442	0.337

Table 3. Shaft diameter estimation.

Fillet radius r_{shaft} [mm]	Shaft diameter d [mm]
0.25	75.9
0.50	73.0
1.00	70.8

$$\sigma_f = k_a k_b k_c k_d k_e k_{f,b} \sigma_f^* \tag{7}$$

$$\sigma_{f,t} = \tau_{sy} = k_a k_b k_c k_d k_e k_{f,t} \sigma_f^* \tag{8}$$

As reported in Tab. 2, different fillet radii are considered in terms of fatigue stress concentration factors: $k_{f,0.50}$ represents a factor's value corresponding to the standard fillet DIN 6885-UNI 6604-69 (31), $k_{f,0.25}$ may be considered instead as depictive of a sharp edge, whereas finally $k_{f,1.00}$ accounts for a fillet increase with respect to the standard suggestions.

By considering a safety factor SF equal to a unit value but at the same time a reliability of 0.99, corresponding to k_c equal to 0.81, the diameters obtained from Eq. 4 are reported in Tab. 3.

The formulation 4, on the contrary of Eq. 3, takes into account the mean and alternate bending and torsional moment contribution, namely M_m, M_a and T_m, T_a. Remembering that the considered shaft diameter equals to 75 mm, it is possible to state that the shaft size is verified according to ASME (26), thus ensuring a shaft unlimited life for the actual loads acting on it.

Table 4. Key shear stress and safety factor obtained.

Variable	Value	
τ_{adm}	240	[MPa]
SF_{key}	4.7	-
$p_{shaft,r=0.50}$	152.5	[MPa]
$p_{hub,r=0.50}$	160.9	[MPa]

Keyway Design Verification

Following the instructions of the standard (*31*), the key dimensions of 20x12x120 mm are checked according to the shaft diameter. To verify the key coupling, the tangential force, the pressure on the key flanks and the shear force present in the key have been estimated as follows:

$$F_t = \frac{T}{r} \tag{9}$$

$$\tau_{key} = \frac{F_t}{bl} \tag{10}$$

$$p = \frac{F_t}{A_{contact}} \approx \frac{F_t}{(l-b)\frac{h}{2}} \tag{11}$$

Comparing the shear force present on the key τ_{key} with the admissible value estimated through Von Mises, the key safety factor is obtained. In Tab. 4 are reported the shear stress present in the key, its admissible shear and the safety factor obtained.

Experimental Evidence

As mentioned at the beginning, this type of crank mechanism is employed in high-torque demanding applications. This article is written to summarise the analyses conducted on the key joints, with particular attention to the crankshaft case study. The reason why a lot of effort was spent in this research activity is resumed in Fig. 2 and 3. Although this shaft seems to satisfy the shaft dimensioning methods present in the literature, as the Design of Transmission Shafting ASME B106.1M (*26*) and its reference articles (*18, 19*), going to be verified for an infinite life, as well as the equivalent analytical stress seems to be not so critical, the shaft breaks.

Experimental Analysis

To validate the correspondence between the analytical, numerical and real shaft stress state during service, experimental tests were carried out. A load cell was used to estimate the thrust force amplitude exerted by the piston, while four strain gages in full-bridge configuration, shown in Fig. 4, were installed on the shaft to measure the shear deformation caused by the torque transmitted. In conclusion, it was possible to record the deformations with reference

Figure 2. Shaft failure section.

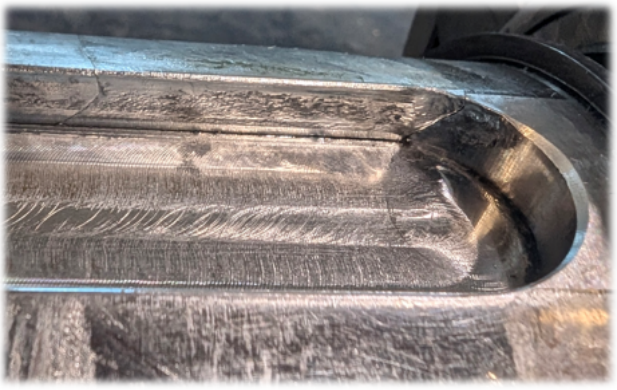

Figure 3. Crack evidence at the base of keyway groove.

to the angular position of the shaft through an encoder. Experimental results highlight how the load and stresses calculated analytically accurately reflect the real operating condition of the crank mechanism, as reported by the torque and thrust force profile comparison figures.

Even if both curve amplitudes present in Fig. 5 and 6 have been divided by the maximum experimental values, the torque and force analytical peaks superimpose with the maximum experimental ones. After this verification, it is possible to state that the analytical nominal stress state well represents the working condition of the shaft. In other words, the nominal stress, calculated analytically, which will be successively multiplied by the stress concentration factors to consider the notch presence, correctly estimates the real stress in the case of a plain shaft.

Figure 4. Part of full bridge strain gages used to measure torque transmitted by the shaft.

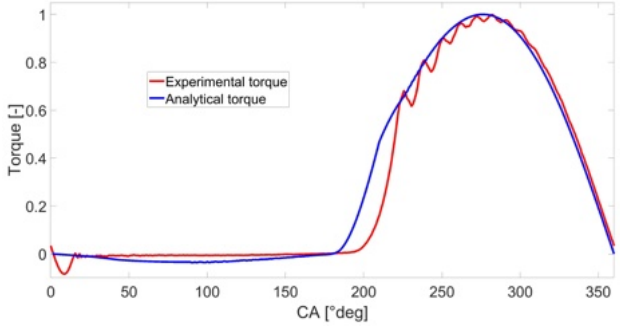

Figure 5. Analytical and experimental torque profile.

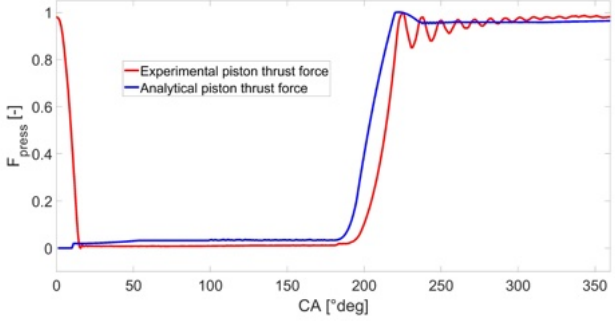

Figure 6. Analytical and experimental thrust force profile.

Alongside this first test type, a dedicated fatigue test rig has been used to reproduce the actual load on the crankshaft. Hence, once the load cycle has been identified through strain gauges, a series of fatigue experimental tests were

Figure 7. Crack nucleation present in a tested shaft.

carried out. Based on the stress present in the FE model, the expected shaft lifespan has been defined in Ch. Shaft fatigue expectations. A series of inspections has been conducted around this threshold, at $5 \cdot 10^4$ and $5 \cdot 10^5$, to check if any crack nucleations occur. As predicted by the FE results along with the fatigue data present in (*32*, *33*), the crack nucleation has been identified in the critical area during the second inspection, namely in the fillet radius at the base of the feather key. Fig. 7 shows the crack present in the tested shafts.

Numerical Models

With the aim of investigating the stress state in the keyway fillet radius, thanks to *Ansys Mechanical*, a series of Finite Element models were built. The numerical analyses conducted could be subdivided into five main blocks based on their objectives. At first, with the aim of identifying the shaft breakage causes, by analysing the loading condition of the considered crankshaft case, employing different hub types, it's possible to determine the bending contribution for different loading conditions. Then, by varying the radial force acting on the concentric hub, the fillet stress state is assessed for a fixed torque transmitted. As third step, for a series of geometries present in previous articles (*10, 11*), the stress concentration factors were estimated through the FE analysis. Instead, to evaluate the frictional effect, the thrust force present on the keyway and the fillet radius' stress variation have been assessed by imposing different frictional coefficients for the standard dimensions reported in (*31*). Finally, a fatigue life estimation has been conducted for a standard keyway (*31*) under the actual load acting on the shaft. This subdivision can be resumed as follows:

- Crank-mechanism keyway bending superposition effect.
- Crank-mechanism keyway variable bending effect.

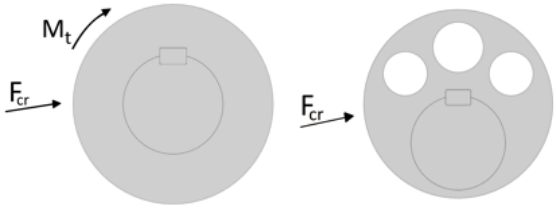

Figure 8. Eccentric model to the right and Hub model to the left.

- Keyway torsional stress concentration factors verification.
- Key force's frictional sensitivity.
- Shaft's fatigue life estimation

Starting from the initial point, the presence of the eccentric intrinsically generates either a torsional and a bending moment on the shaft. In this configuration, by applying a force along the connecting rod direction on the eccentric external surface, as reported on the right side of Fig. 8, it is possible to reproduce exactly the loading condition both on the shaft and through the key coupling. To better identify the bending contribution in the fillet prismatic keyway portion, a second model was created by substituting the eccentric with a simple concentric hub, as shown on the left side of Fig. 8. In this second model, the torsion and bending moment can be easily separated since they depend, in this case, on the torque and radial force applied to the concentric hub respectively. Thereby, keeping the torque applied and loading or not the hub with the connecting rod force, was possible to estimate, thanks to the difference in stress states, the bending effect. For these three models, as reported in Ch. Crankshaft dimensioning verification to fatigue and Analytical Models, three different fillet radii were considered. Special attention has been given to the prismatic part of the keyway, more specifically to the fillet radius at the base of the feather key groove.

To fulfil the second point, by employing the concentric hub model, for a fixed amount of torque transmitted, the stress state in the reference point S_c (as depicted in Fig. 10) has been estimated for a variable radial load acting on the hub. The geometry considered in this analysis corresponds to r_{shaft} equal to 0.50 mm.

In parallel to these two sections dedicated to the crank mechanism analysis, another series of numerical simulations was conducted. The previous sections, which are dedicated to the crankshaft case study, are more prone to understanding the effects of combined loads and fillet radii. Here instead, the objective is to validate through FEM analysis the most recent stress concentration factors present in literature, which were estimated in the past thanks to photo-elasticity. The geometries considered are representative of the ones used in

Figure 9. Feather key forces.

the references, so, for every article treated, the geometry has been set accordingly.

As the fourth point, based on the tangential force variation to which the key is subjected, the frictional effects have been considered in the case of an eccentric hub. Thus, by applying different friction coefficients, the load share over the key has been assessed both in terms of keyway stress and also by the force transmitted through it. For this last case study, the eccentric hub configuration has been chosen to ensure a fixed ratio between the torque and the radial load present in the hub-shaft coupling. A different friction coefficient causes not only a tangential force variation coming from the hub, but below a limit value, the key becomes free to rotate inside its seat. To describe this phenomenon, the forces represented in Fig. 9 have been estimated for different friction coefficients, from zero to 0.2.

Finally, as a last step, according for example to (*36–38*), a fatigue life estimation has been assessed for a standard keyway, by employing a fillet radius equal to 0,50 mm as suggested by the standard (*31*). Thanks to the eccentric model used in point two, the stress along the keyway fillet is estimated for a series of crankshaft positions involved in the compression stroke. By applying a nodal selection along the keyway length, the stress tensor at each node is extracted. Once the stress variation along the cycle is obtained, an appropriate failure criterion is adopted to esteem the shaft fatigue life.

Keyway Groove Geometries

For the crankshaft case study, based on the standard (*31*), a series of geometrical modifications have been performed on the keyway fillet radius r_{shaft}, as reported in Fig. 10. The aim is to observe the stress trend depending on the key groove fillet radius r_{shaft} for a standard metric keyway. The length of the feather key is kept as a constant parameter, as well as the key and keyway's height h, as reported in Tab. 5.

On the other hand, for the stress concentration factors verification, a diameter of 75 mm is maintained, while the keyway geometries, such as depth, width, and fillet radius, are sized according to the ratio present in the reference articles.

Table 5. Key quotes.

Key quote	Value [mm]
h	12
b	20
l	120

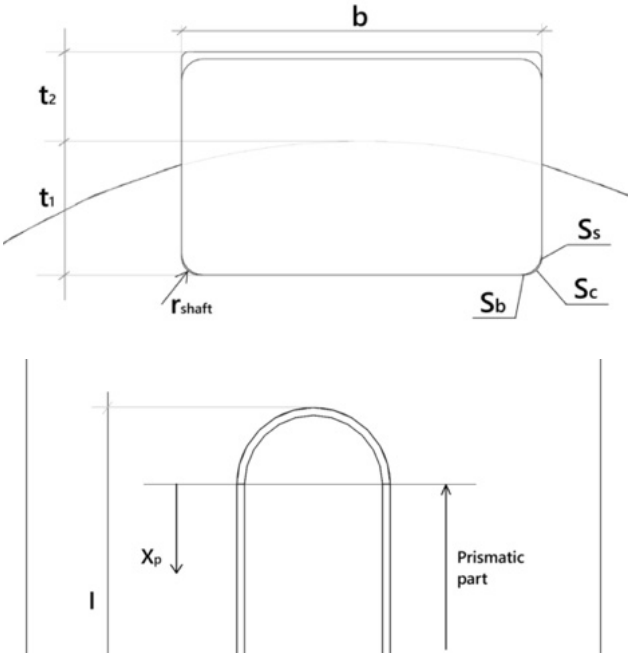

Figure 10. Feather Key quotes.

Constraints and Forces

Regarding the crankshaft case study, in $Ansys$, the constraints were set by referring to a cylindrical coordinate system: two axes are placed in the axial and radial direction of the shaft while the third angular coordinate is used as a degree of freedom to permit or to lock the shaft rotation. Referring to Fig. 11, the bearing named as R_A constraints the radial and axial directions, while bearing R_B, which represents a cylindrical roller bearing, locks only the radial displacement. To blind the rotation of the shaft, a third constraint R_θ is applied in the major cross-section diameter. With these support settings, the shaft rotation along the y and z axes is however tied in these shaft portions. To have coherence between the analytical and FE values adopted in Eq. 19, the bending moment from which K_{flex} was estimated derives from an $Ftool$ model in which these supports are not orientable. Depending on which of the three models, the connecting rod force is applied on the eccentric external surface or, in the concentric hub case, an equivalent torque alone or in combination with the connecting rod force is applied. In the first case, as previously stated, by applying

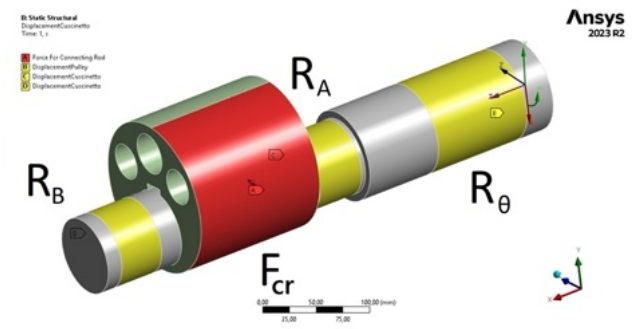

Figure 11. Ansys model with loads and constraints applied.

just a force on the eccentric, the shaft remains subjected by either bending and torsional moment. Either for the variable bending effect study but also for the numerical stress concentration factors estimation, the concentric hub-shaft model setup described before have been used.

Contact and Mesh Resolution

To address the contact issue between the three bodies, specific mesh sizes and surface contact roles have been set. The models used are consistent with the nominal components' dimensions, so no tolerances have been taken into account in the FE results. The mesh is defined by tetrahedral second order elements, and the number of nodes depends on the feather key radius, with an average of 1,5-2 million of nodes for each model considered. A mesh sensitivity analysis leads to setting a series of mesh refinements, especially in the keyway fillet radius and in the surrounding areas. The mesh sizes present in the models are summarised in Tab. 6. In both contacts with the shaft and the eccentric, the key has to be chosen as the target body for its concave shape, consequently, both keyway grooves possess a contact surface definition. Following the same criterion, the shaft and the eccentric surfaces are defined as contact and target respectively. In order to fulfil the contact requirement, for every contact pair, a finer mesh is applied on the target side. To conclude, a pinball region is set to ensure contact only on the interested surfaces and not in the fillet at the base of the key groove.

For the crankshaft studies, for every contact pair, a friction coefficient μ_s equal to 0.11 is set, with reference to (*35*), to reproduce the steel-steel friction in the presence of oil. On the other side, for the validation of the torsional stress concentration factor K_t, the friction coefficient is set in accordance with the reference papers. As reported in Par. Key Frictional Sensitivity, μ_s plays a fundamental role in determining the additional contribution that comes from the key rotation. For the specific case study treated in the next paragraph, 0.11 turns out to be the friction threshold for which the key rotation doesn't affect (as experimentally highlighted) the actual load perceived by the shaft's keyway. On the other side, for the validation of the torsional stress concentration factor K_t, the friction coefficient is set in accordance with the reference papers.

Table 6. Mesh refinements.

Zone	Mesh size [mm]
Key sides	0.7
Keyway sides	0.8
Keyway fillet radius	0.1
Eccentric keyway sides	2
Eccentric hole	7
Shaft lateral surface	5

Results Evaluation

Either for the case study, but also to verify the stress factors from FE results, through the probe tool, the nodal stress state has been estimated in the three considered points of Fig. 10. In this way, the stress tensor has been reconstructed and, by writing it back according to a primary triad reference system, the principal stresses have been obtained. To identify the maximum shear stress present in the fillet, in accordance to (*8–11*), a Mohr circle rule has been adopted and reported in Eq. 12 for the calculus of τ_{max}.

$$\tau_{max} = \frac{\sigma_1 - \sigma_3}{2} \tag{12}$$

Analytical Models

In the analytical analysis, the shaft is treated as an isostatic beam where, for every shaft cross-section and for every crank angle position, the nominal stress state for a plain shaft has been estimated. The so-called stress concentration factors enable the computation of the actual notch stress state based on the nominal stress present for the same solid shaft. These coefficients, in particular the ones referred to the keyway, have been defined in the past through different methods like photo-elasticity and electro-coating. The photoelastic oldest studies like (*12*) had considered an empty keyway, while a series of papers published in the 80s' report the stress concentration factors for a key transmitting torque. In accordance with the notch geometry and the shaft' nominal stress, a discrepancy shone through when the analytical local stresses were compared to FE model result. This difference led to the verification of the stress concentration factors present in the literature by reproducing, via FE, the photoelastic models used in the most recent articles.

Nominal Stress State

To characterize the nominal stress over a cycle, the shaft has been modelled in $Matlab$ as an isostatic supported beam with distributed loads and constraints as represented

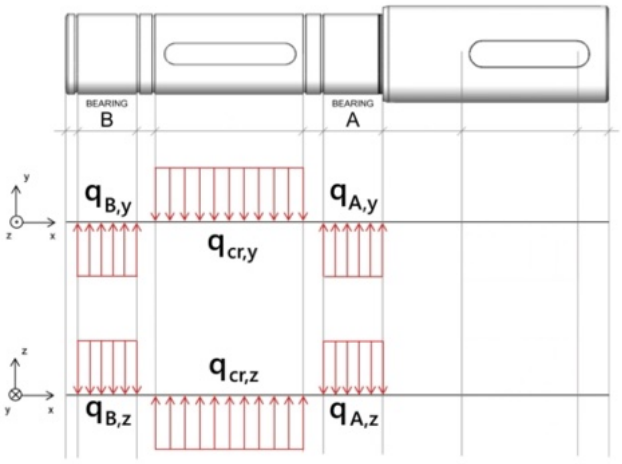

Figure 12. Non-conventional crank mechanism free body diagram.

in Fig. 12. The connecting rod force F_{cr} was considered as a time variable since the pressure over the piston top and the connecting rod angle vary over the pumping cycle. By imposing the equilibrium conditions for each shaft cross-section and each crank angle, the shear τ_t and the normal stress σ_b have been estimated for a plain shaft (by using a tailored Matlab script). The analytical steps are covered more comprehensively in (*30*). In particular, the nominal stress state has been assessed through Eq. 13, 14, 15 and 16 for the most stressed crank angle position, corresponding to the middle of the compression stroke. Moreover, by considering the entire load cycle, thanks to a reference system fixed with the shaft, was possible to define the average and alternating stresses at every shaft point [†]. Fig. 13, 14 and 15 represent the shear due to torsion, the normal stress due to bending and the equivalent Von Mises stress at the middle of the compression stroke, when both reach their maximum amplitude. The nominal stress state is expressed in a non-dimensional form, dividing it by the shaft fatigue limit in case of 10^6 cycles. In the present work, the shaft fatigue limit σ_b has been set equal to 329 MPa (*32*, *33*)[‡]. The shaft nominal stress has been used as a reference point for all the different types of analysis conducted. The nominal values of torsion and bending coming from the strain gauge experiments were used to verify either the analytical results but also to validate the various numerical models used.

$$\sigma_b = M_b y / I_x \tag{13}$$

$$\tau_t = M_t r_i / I_p \tag{14}$$

$$\tau_s = 4T / 3\pi r^2 \tag{15}$$

$$\sigma_{eq} = \sqrt{\sigma_b^2 + 3\tau_t^2} \tag{16}$$

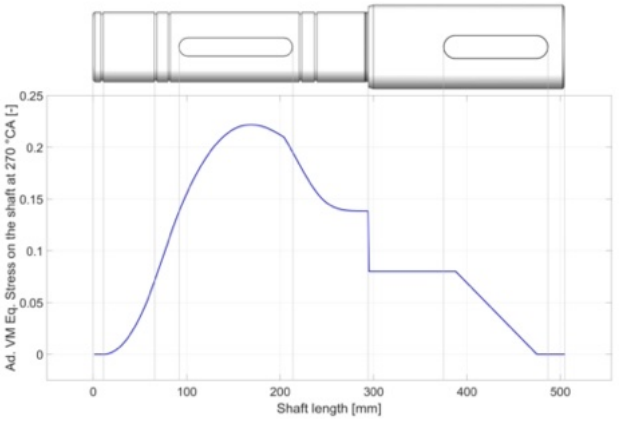

Figure 13. τ_t along the shaft for 270 $^\circ CA$.

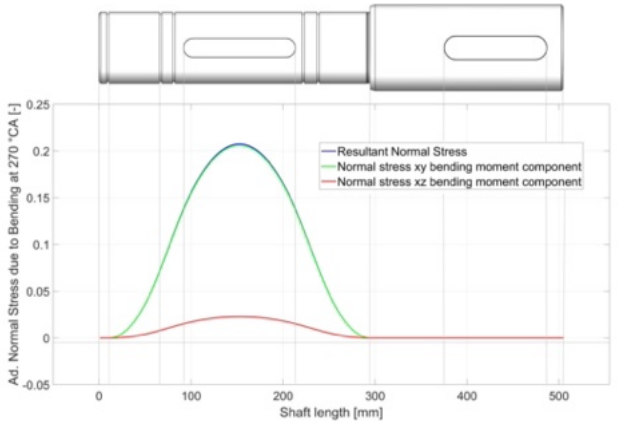

Figure 14. σ_b along the shaft for 270 $^\circ CA$.

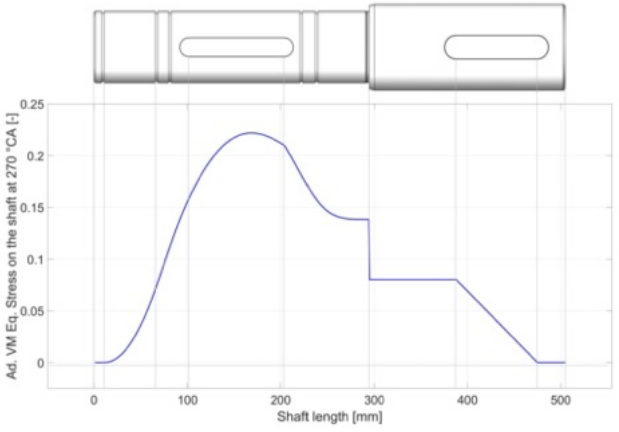

Figure 15. σ_{eq} along the shaft for 270 $^\circ CA$.

[†]Complete analysis present in (*30*).
[‡]39NiCrMo3 fatigue data present in (*32*).

Notch Effect for Loaded Key

Initially, the torsion stress concentration factors for keyways have been estimated by imposing loads and constraints far away from the notch neighbourhood. These loading conditions do not reflect the real stress state of a torque-transmitting keyway. However, more recent articles overcome this initial simplification by applying a torque directly through the key. Different techniques have been used to obtain this multiplier factor in keyways: Ōkubo et al. (16) uses the electro-coating method over small-diameter shafts, while Fessler and Eissa (8, 9, 10, 11) reports the stress state variations observed over photo-elastic prototypes. Regarding the pure torsional stress, by retracing the definition of stress concentration factors K_t present in previous papers, two references have been set: a first reference is defined as the surface torsional stress for an equivalent plain shaft, while the second corresponds to the mean shear stress present in the key, as reported in Eq. 17 and 18. Since τ_{max}, by its definition, refers to the difference between principal stresses σ_1 and σ_3, its value remains affected by the presence of bending. For this reason, the results inherent to the first section, which is dedicated to the combined loading condition, are expressed only in terms of K_{ts} and K_{tk} even if not all the models deal with mere torsion. This type of comparison would be seen as a first estimation of the bending effect over the total stress in the fillet.

$$K_{ts} = \frac{\tau_{max}}{\frac{16T}{\pi d^3}} \tag{17}$$

$$K_{tk} = \frac{\tau_{max}}{\frac{2T}{dbl}} \tag{18}$$

On the other hand, as regards the crankshaft case study, to provide a comparison with the finite element results, both analytical and numerical outcomes refer to the same crankshaft position. Taking as a reference the behaviour of the piston thrust force and the torque profile over a cycle, with reference to Fig. 5 and 6, it is possible to identify on one side the torque peak angular position, whereas, on the other side, the piston force constant trend over the pumping phase. The middle point of the compression stroke, indeed 270 $°CA$, where both torsion and bending stresses are maximum, constitutes the most stressed position of the shaft, and this is why it was selected as a reference. Even though this crank angle surely corresponds to the most stressed shaft position, being the bending moment neutral plane passing through the middle of the key (more precisely, is normal to the connecting rod axis), the maximum bending stress is detected not in the keyway region but is located on a shaft surface point with an offset of 90°. With regard to the aforementioned, the top dead center position was not considered as the most stressed keyway position since just the bending contribution doesn't provide a stress in the fillet as high as for the combined case. Despite the effective bending stress acting in the keyway fillet is affected by this distance reduction, the stress concentration $K_{t,flex}$, which has been estimated from the second blocks of analyses, is referred to the shaft nominal bending stress present in section X_p as reported in Fig. 14.

So, to reasonable estimate a bending stress concentration factor in case of combined bending and torsion, the Tresca equivalent stress definition was deemed: by combining the Tresca equivalent for a tridimensional stress state with the one in case of planar stress (*34*), a multiplied factor $K_{t,flex}$ could be attributed to the shaft nominal bending stress alone σ_{yy}.

$$2\tau_{max} = \sqrt{K_{t,flex}^2\sigma_{yy}^2 + 4K_{t,tors}^2\tau_{xy}^2} \tag{19}$$

By looking at Eq. 19, two times τ_{max} refers to the tridimensional equivalent stress while the second portion of the equation reports the Tresca equivalent in case of planar stress. The two quantities τ_{xy} and σ_{yy} result to be the nominal shear and bending stress respectively in case of plain shaft. Considering a pure torsion load case, Eq. 19 could be simplified, obtaining in this way the definition of stress concentration factor present in Eq. 17 or, by substituting τ_{xy} with the shear present in the key and its relative coefficient K_{tk}, Eq. 18.

Fatigue Life

To estimate the shaft's fatigue behaviour, the eccentric model has been adopted for its versatility to consider different crankshaft angular positions. In this way, after discretising and numerically solving the complete shaft duty cycle, it was possible to recompose a stress tensor for each node of interest at every angular position of the crank. A collection of one hundred and thirty-six nodes has been selected at the medium fillet radius point S_c, along the prismatic keyway portion. Having resumed in a tabular manner the stress tensor components possessed by each node during the cycle, becomes possible to perceive the trend and the stress amplitude necessary to choose a proper fatigue criterion. As a double check, thanks to the vectorial representation of the principal tensor components, the absence of direction's variation with respect to the shaft tied coordinate system was verified. The maximum principal stress direction is constantly oriented tangent to the fillet radius in the node of interest. One only minor change happens around 160 $°CA$, when the set of nodes start to perceive along the same tangent direction a negligible compressive state, while the maximum principal becomes equal to zero. Based on the tensor behaviour described above, a Sines failure criterion (*22*) is selected to forecast the fatigue behaviour of the feather key. After obtaining the stress principals maximum and minimum values, the equivalent alternate and medium stress following Sines have been obtained thanks to Eq. 20 and Eq. 21.

Table 7. Specimen fatigue data, R=-1. (*32, 33*)

Nr. of cycles	Stress Amplitude [MPa
10^3	838
10^4	719
10^5	617
10^6	530
10^7	455

$$\sigma_{eq,alt} = \frac{1}{\sqrt{2}}\sqrt{(\sigma_{a,1}-\sigma_{a,2})^2+(\sigma_{a,1}-\sigma_{a,3})^2+(\sigma_{a,2}-\sigma_{a,3})^2} \quad (20)$$

$$\sigma_{eq,avg} = \sigma_{m,1}+\sigma_{a,2}+\sigma_{m,3} \quad (21)$$

On the other side, thanks to the fatigue data present in (*32*), the shaft Haigh diagram have been composed considering the coefficient k_a, k_b and k_c present in Tab. 2. Afterwards, for each nodal means stress $\sigma_{eq,avg}$, the alternate fatigue limit have been gained looking at Haigh. Passing to the Wohler diagram specific to each nodal mean stress, the expected nodal life cycle has been obtained starting from the alternate equivalent stress $\sigma_{eq,alt}$. The specimen fatigue values obtained from (*32, 33*) are resumed in Tab. 7.

Results

As described in Ch. Numerical Models and Analytical Models, the stress states in the keyway fillet have been defined following analytical and numerical methods. For the shaft case study, by employing different models, a reliable estimation of the fillet stress has been accomplished, either for pure torsion but also in the case of bending superposition. In addition, the torsional stress concentration factors present in the literature have been verified thanks to FE and lastly, the effects of friction.

Bending Superposition Effect in Keyway

To estimate the bending contribution and at the same time assess the fillet radius influence for the considered crankshaft case study, different hub types and several fillet radii have been considered. The presence of the eccentric, as presented in Fig. 11, by subdividing the force along the conrod into bending and shear stress acting on the shaft, doesn't permit decoupling the two contributions. For this reason, a second model was defined, going to replace the eccentric with a concentric hub. In this way, it became possible to separate these effects, having in this case the nominal torsional stress as a function of the torque and the nominal bending stress dependent on the radial force applied to the hub.

As mentioned previously, in this section, the effect of fillet radius has been estimated thanks to three different values. To resume, the radius equal to 0.50 mm represents the standard suggestion (*31*), 0.25 mm depicts the absence of fillet (since, as usual, each end mill possesses a minimum curvature even if it is declared as a sharp edge mill), and finally the one-millimeter radius aims to appreciate the effects of an increment compared to the standard. Three inspection points have been selected according to Fig. 10 and, for the sake of simplicity, the results reported in Tab. 8, 9 and 10 refer to a distance X_p fixed to $0.05d$, which corresponds to the most stressed point of the keyway fillet radius.

Table 8. Stress Concentration factors K_{tk} for S_c point

Models Fillet Radius	Hub Pure Torsion	Hub Torsion & Bending	Eccentric
0.25	11.7	14.6	15.3
0.50	8.8	10.7	11.6
1.00	6.5	7.7	8.3

Table 9. Stress Concentration factors K_{tk} for S_s point

Models Fillet Radius	Hub Pure Torsion	Hub Torsion & Bending	Eccentric
0.25	10.5	12.9	13.9
0.50	7.7	9.6	10.7
1.00	5.5	6.7	6.7

Table 10. Stress Concentration factors K_{tk} for S_b point

Models Fillet Radius	Hub Pure Torsion	Hub Torsion & Bending	Eccentric
0.25	11.1	12.7	12.3
0.50	8.0	9.2	10.0
1.00	5.3	6.2	6.0

It has been chosen to report in Tab. 8, 9 and 10 only the stress concentration factor K_{tk} but in any case is possible to recover the respective value of K_{ts} going back to Eq. 17 and 18.

As the tables show, a higher K_{tk} has been estimated for the combined torsion-bending cases: this implies that the maximum shear stress τ_{max} results, as expected, to be affected by bending. To overcome this condensation of bending and torsion over the same coefficient, in the next section, a stress concentration factor devoted to bending only has been assessed.

Keyway Variable Bending-Torque Effect

As previously mentioned, a second group of models has been developed to monitor the stress behaviour during the shift in torque-radial force ratio. This study has been conducted by exploiting the concentric hub model considered in the previous section. Differently from the first branch of analyses, here, for a constant torsional moment applied, different loading conditions have been established by varying the radial force acting on the hub. The fillet radius adopted for this parametric study corresponds to 0.50 mm while

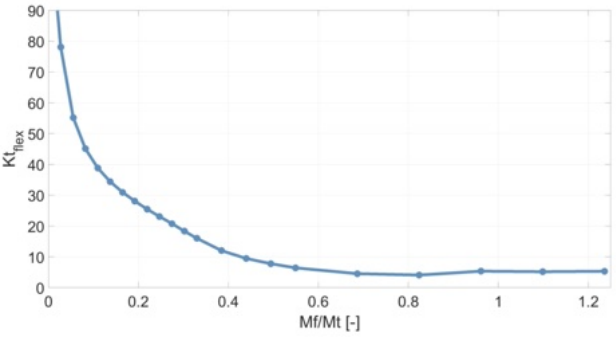

Figure 16. Stress concentration factor for bending for a variable bending-torque ratio.

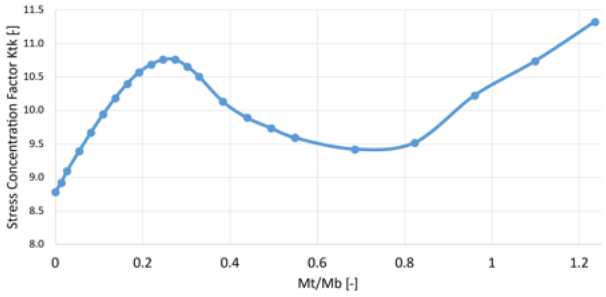

Figure 17. Stress concentration factor K_{tk} for variable hub radial force estimated in S_c point.

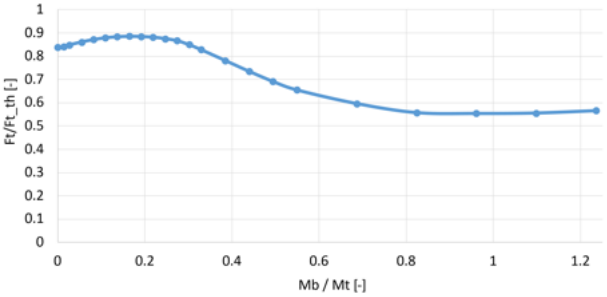

Figure 18. Tangential force F_t applied on the prismatic keyway side.

S_c represents the point in which the stress state has been estimated. For the majority of load cases the maximum stress in the fillet has been observed for X_p about 0.05, but when the ratio between bending and torsion goes beyond 0.5, the maximum stress perceived moves toward the end milled portion of the keyway, reaching in this way an even lower value of X_p.

Going back to Eq. 19, thanks to the first load case in which pure torsion is applied, the value of $K_{t,tors}$ and τ_{xy} have been set. The other parameters like τ_{max} and σ_{yy} instead have been collected and inserted in the equation for each remaining load case. The nominal bending stress σ_{yy} has been estimated analytically on the X_p cross-section as a consequence of the radial force applied. As the last step, by inverting Eq. 19, the values of $K_{t,flex}$ are retrieved. In Fig. 16 the trend of the bending stress concentration factor is presented for a variable ratio between the bending moment and torsion.

The variation of the stress state as a function of the bending-torque ratio could also be expressed in terms of just one stress concentration factor, as was done for the superposition effect results. The same stress state from which $K_{t,flex}$ has been extracted is presented in terms of K_{tk} in Fig. 17. On the other side, to have a more complete insight of the stress variation causes, the normal force exerted on the prismatic surface of the keyway is reported in Fig. 18. This key thrust force is expressed as a ratio with the nominal tangential force F_t estimated by Eq. 9.

Literature Stress Concentration Factors

Based on the high K_t outcomes coming from the crankshaft FE model, a series of CAD geometries have been created with the aim of verifying the stress concentration factors present in literature. Among the papers, four models have been selected: from (*11*), following the metric standard, by considering different ratios between the length of the key and the shaft diameter, three keyway geometries have been replicated; on the other side, from Fessler and Eissa (10), the named $5m$ model was considered with its fixed d/l ratio. In this lineup, the shaft's diameter has been kept consistent with the one present in the first two analysis sections.

Table 11. Literature stress concentration factors geometries.

Parameter		Models 1 - 2 - 3	Model 4
Hub length	l	$0.5d$ - $1d$ - $2d$	$2d$
Key Width	b	$0.286d$	$0.286d$
Key Thickness	T	$0.160d$	$0.172d$
Fillet Radius	r	$0.010d$	$0.010d$

In the same way as for the crankshaft case study, by performing numerical analyses on the four different models associated with dimensional ratios specified in Tab. 11, it was possible to compare the literature K_t values with those resulting from FE. By reconstructing the stress state for the points S_c, S_s and S_b in the so-called stress tensor, the maximum principal stresses have been estimated by imposing the matrix determinant equal to zero. Along the keyway, those points have been selected with a ratio X_p/d about 0.05, where the stress in the fillet radius reaches its maximum. Once τ_{max} is defined with Eq. 12 as for the case study, thanks to Eq. 17 and 18, the stress concentration factors K_t were obtained, in the same way as (*10, 11*). Following these steps and foresights, Tab. 12, 13, 14 and 15 resume respectively the numerical and photoelastic K_t values for each model considered. The maximum principal stress distribution in the keyway neighbourhood is represented in Fig. 19.

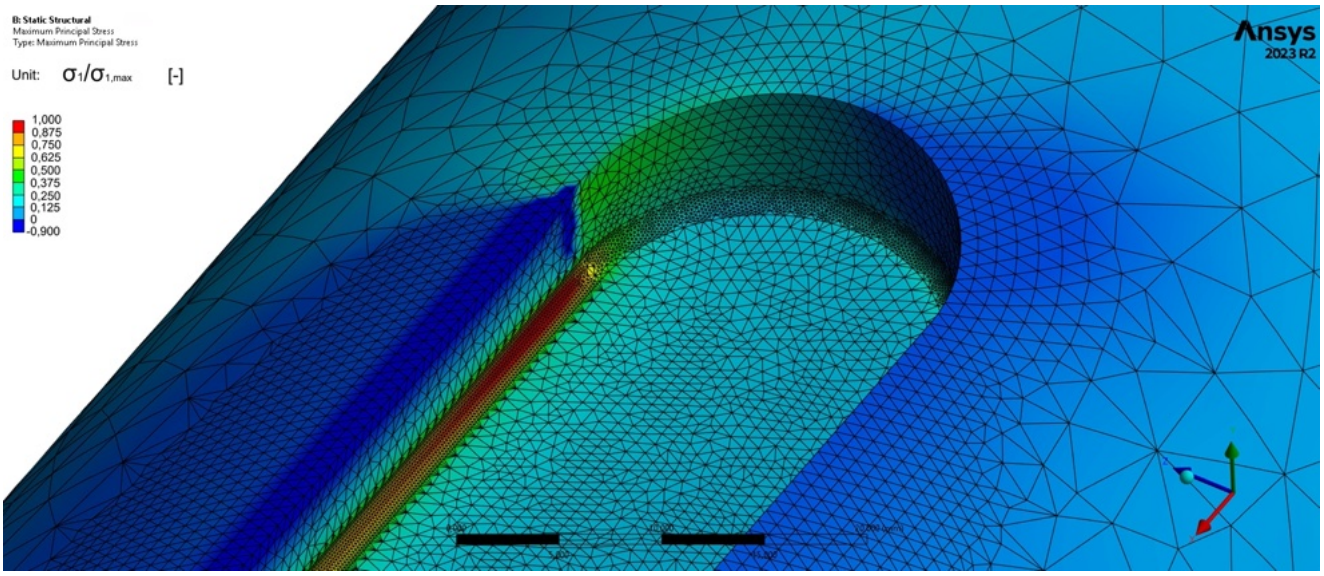

Figure 19. Maximum principal stress distribution in the keyway neighbourhood.

Table 12. Stress Concentration Factor K_{ts} for Model l/d=2 Fessler and Eissa (10).

Point of inspection	FE model	Photo-elastic model (*10*)	Increment [%]
S_s	5.2	4.1	26.1
S_c	5.8	-	42.2
S_b	5.2	2.9	78.7

Table 13. Stress Concentration Factor K_{ts} for Model l/d=2 Fessler and Eissa (11).

Point of inspection	FE model	Photo-elastic model (*11*)	Increment [%]
S_s	5.3	4.0	32.3
S_c	5.8	-	44.0
S_b	5.1	3.1	64.7

Table 14. Stress Concentration Factor K_{ts} for Model l/d=1 Fessler and Eissa (11).

Point of inspection	FE model	Photo-elastic model (*11*)	Increment [%]
S_s	7.8	6	30.0
S_c	10.0	-	66.3
S_b	7.8	4.2	85.7

Table 15. Stress Concentration Factor K_{ts} for Model l/d=0.5 Fessler and Eissa (11).

Point of inspection	FE model	Photo-elastic model (*11*)	Increment [%]
S_s	14.5	10.5	37.6
S_c	20	-	90.5
S_b	15.5	7.5	106.6

Key Frictional Sensitivity

Since the working condition of the shaft normally includes either a torque but also a radial load present in the hub-shaft interface, the effect of friction becomes relevant in terms of tangential force exerted through the key. By adopting the previous $Eccentric\ Model$ with a keyway fillet according to DIN 6885-UNI 6604-69 (31), the frictional effects have been estimated in terms of force exchanged by the key and evaluating the stress in the S_c point. Regarding the key, the tangential force coming from the hub and transferred to the shaft creates an unbalance in terms of moment. Thus, in addition to diminishing the tangential force, the friction also prevents the key's rotation in the shaft seat, caused by this moment disequilibrium. For a fixed amount of force applied to the eccentric, the major forces that are created around the key, presented in Fig. 9, have been estimated for different friction coefficients.

As highlighted in Fig. 20, for μ_s which tends to zero, the discrepancy between the force coming from the hub F_{hub} and the one transmitted to the keyway thrust side F_{kw} grows. At the same time $F_{kw,th}$ reaches its maximum for the absence of friction, while it tends to zero for a μ_s higher than 0.11. In other terms, the key's rotation results in an ulterior force $F_{kw,th}$ that is added to the tangential one already exerted by the hub F_{hub}. For this reason, the dimensionless ratio between F_{kw} and F_{cr} reaches a value higher than a unit in the case of low friction coefficients. At the same time, as soon as the additional force $F_{kw,th}$ vanishes, the tangential forces of the hub F_{hub} and of the shaft F_{kw} converge. To better appreciate the variation of keyway rotation in case of different friction coefficients, Fig. 21 reports the key' displacements with the same deformation scale of 2.5 for μ_s equal to zero and 0.2.

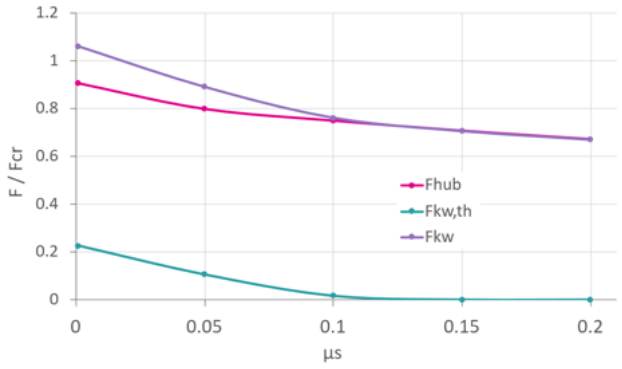

Figure 20. Variation of the keyway hub tangential force F_{hub}, tangential force exerted on the shaft keyway support side F_{kw} and opposite side $F_{kw,th}$.

Lastly, to represent the stress state τ_{max} present in the inspection point S_c, the stress concentration factors K_{tk} have been estimated and resumed in Fig. 22, where the only parameter μ_s varies. The K_{tk} trend beside Fig. 20 reveals the direct dependency between the total tangential force perceived and the resultant stress. In other terms, once the friction threshold is passed, the effect of friction becomes relevant only for F_{hub} while $F_{kw,th}$ remains fixed to zero. At the same time, below 0.11, the K_{tk} slope tends to increase as a consequence of a dual contribution: further to the tangential force coming from the hub, the key starts to rotate, exerting in this way the additional force $F_{kw,th}$.

Shaft fatigue expectations

Based on the complete duty cycle analysis, the Sines' invariant criterion has been chosen as appropriate to estimate the fatigue life expectancy for the keyed shaft. Inserting the mean equivalent stress and then the alternate equivalent stress on the Haigh and Wohler diagrams respectively, the expected fatigue cycles have been assessed for each S_c point as the x_p coordinate varies. The resultant expected fatigue life associated to each node is presented in Fig. 23. The green and orange lines account for the test bench experimental evidence reported in Ch. Experimental Analysis.

Conclusions

In the present work, starting from the experimental evidence, the shaft's fracture causes have been searched among analytical, experimental and numerical analyses. As a starting point, the shaft dimensioning standard aids in ruling out a possible underestimation of the shaft diameter, which could have occurred during its design phase. By adopting the corrective factors, especially the literature stress concentration ones, reported in Tab. 2, the shaft seems to satisfy the diameter suggested by ASME (26) for any fillet radius accounted.

On the other side, thanks to the experimental strain gauges activities, the effective loads acting on the shaft have been verified under real operational conditions. In this way, the nominal stresses, which are the basics for the analytical analyses, have been confirmed.

The first set of analysis dedicated to the superposition shows the bending effect over τ_{max}. By resuming its definition, τ_{max} not only reflects the maximum shear present in the keyway, as the presented in Mohr circles but, since it is based on the difference between the maximum and minimum principal stresses, it feels the effect of bending over the keyway fillet, as expressed more explicitly by the Tresca planar failure criterion.

In turn, by performing parametric studies for different bending-torque ratios, it emerged a non-linear stress state variation in the fillet. From a point of view of τ_{max} and K_{tk}, it seems that for a ratio around 0.25 the stress reaches a local maximum. It can be explained by a still high tangential force acting on the keyway thrust side. Going to increase the bending contribution, after a minima caused by frictional forces, the stress rises again linearly, probably due to the deflection of the shaft, which condensates the tangential force at the extremity of the key, near its end milled portion. Alongside the effects of different bending torque ratios and as proof of what was assumed with respect to the trend shown in Fig. 17, the friction coefficient also contributes to a variation in terms of tangential force and then in the stress present in the fillet radius.

The fundamental point for which the shaft failure can be explained are the stress concentration factors K_{ts} and K_{tk} present in the literature. Those multiplier indexes, being present either in the shaft dimensioning standard (*26*) but also in the analytic calculus for the effective stress present in the notch, could inevitably compromise the shaft design and consequently its fatigue life prediction. Observing the photo-elastic and the FE models coefficients K_{tk} present in Tab. 12, 13, 14 and 15, it is evident how the literature coefficients reveal a stress state lower compared to the numerical one. Besides, this discrepancy is enhanced for older publications, by which these underestimated values of K_t could be reported in some stress concentration factor textbooks as correct. As a proof, the fatigue life estimation according to Sines shows a limited number of cycles corresponding to the experimental failure point showed in Fig. 7. In light of these results, a last comment should be made with regard to the actual key standard. The fillet radii suggested, at least for the considered case of a 75 mm diameter shaft, combined with the literature keyway coefficients, can provoke an untimely, not predicted shaft failure. In conclusion, for the sake of safe design, this experience suggests designing the keyway according to the standard, but checking it with a numerical model, in order to properly estimate the stress field.

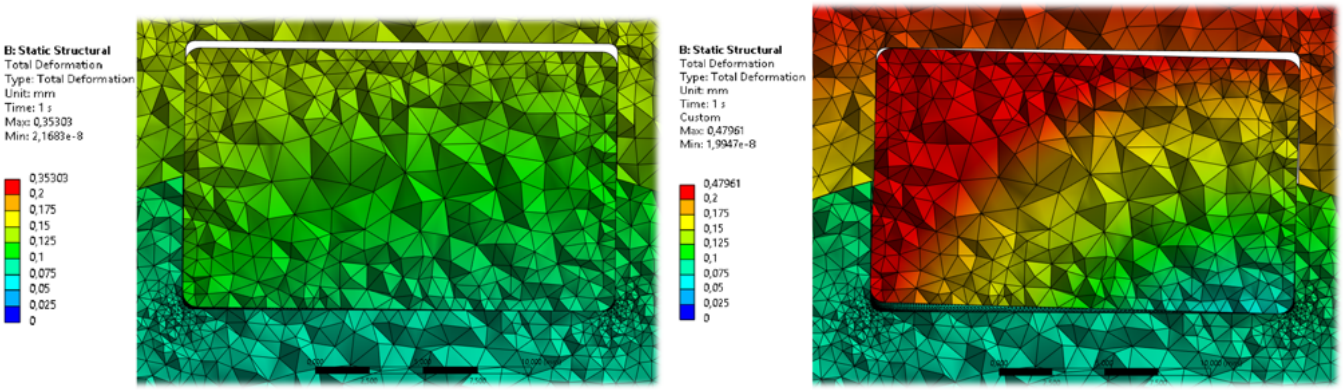

Figure 21. Frictionless key displacement on the left and μ_s=0.2 key displacement on the right, deformation scale 2,5x.

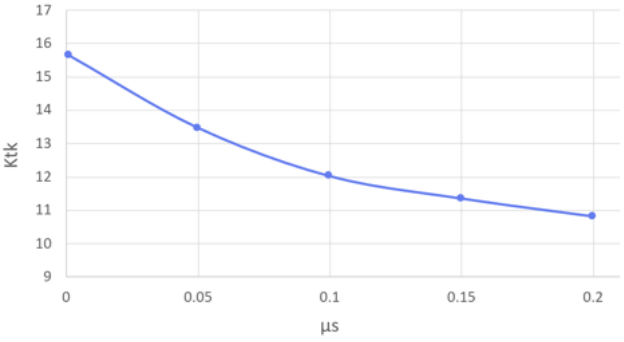

Figure 22. K_{tk} variation for different friction coefficient μ_s.

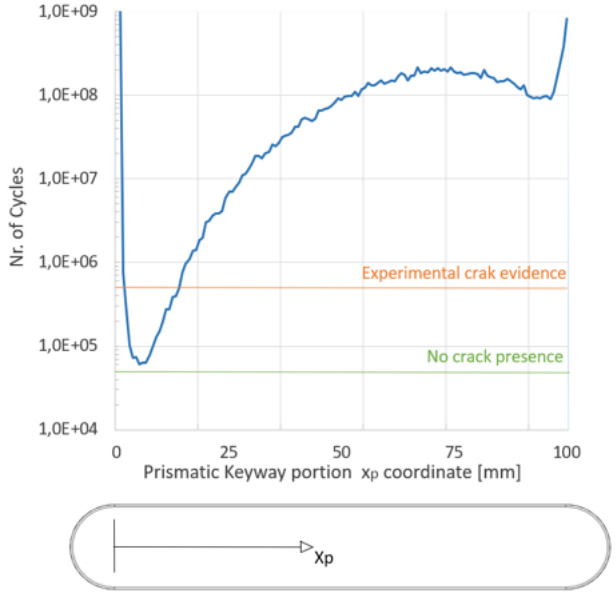

Figure 23. Fatigue life expectation according to Sines for S_c points along x_p coordinate.

Acknowledgements

The authors thank the Politecnico di Torino and the Department of Mechanical and Aerospace Engineering for providing the necessary facilities.

Prepared using TRR.cls

References

1. L. Filon. On the resistance to torsion of certain forms of shafting, with special reference to the effect of keyways. *Proceedings of the Royal Society of London*, 65:428–432, 1899.
2. H. F. Moore. *The effect of keyways on the strength of shafts*. Number 42. The University, 1909.
3. T. Gronwall. On the influence of keyways on the stress distribution in cylindrical shafts. *Transactions of the American Mathematical Society*, 20(3):234–244, 1919.
4. W. Shepherd. The torsion and flexure of shafting with keyways or cracks. *Proceedings of the Royal Society of London. Series A, Containing Papers of a Mathematical and Physical Character*, 138(836):607–634, 1932.
5. H. Ōkubo. On the torsion of a shaft with keyways. *The Quarterly Journal of Mechanics and Applied Mathematics*, 3 (2):162–172, 1950.
6. M. Eissa. Elastic stress concentrations in side milled hollow and solid keyed connections. *The International Conference on Applied Mechanics and Mechanical Engineering*, 1:45–54, 5 1984. ISSN 2636-4360. doi: 10.21608/amme.1984.48833. URL https://amme.journals.ekb.eg/article_48833.html.
7. H. Fessler and T. Appavoo. On the effect of key edge shape on keyway edge stresses in shafts in torsion. *The Journal of Strain Analysis for Engineering Design*, 24(3):121–125, 1989.
8. H. Fessler and M. Eissa. Elastic stresses due to torque transmitted through the prismatic part of keyed connections part i: Effect of different fits and friction on standard shapes. *The Journal of Strain Analysis for Engineering Design*, 17(2):103–111, 1982.
9. H. Fessler and M. Eissa. Elastic stresses due to torque transmitted through the prismatic part of keyed connections part ii: Effect of shape with usual fits and friction. *The Journal of Strain Analysis for Engineering Design*, 17(4):215–222, 1982.
10. H. Fessler and M. Eissa. Reduction of elastic stress concentrations in end-milled keyed connections: A frozen-stress photoelastic analysis of keys, shafts and hubs with end-milled keyways loaded by torque transmitted through the

key. metric and inch standard keys were modified to reduce maximum stresses in the shaft. *Experimental mechanics*, 23: 401–408, 1983.
11. H. Fessler and M. Eissa. Three-dimensional, elastic stress distribution in end-milled, keyed connections. *The Journal of Strain Analysis for Engineering Design*, 18(2):143–149, 1983.
12. H. Fessler, C. Rogers, and P. Stanley. Stresses at end-milled keyways in plain shafts subjected to tension, bending, and torsion. *Journal of Strain Analysis*, 4(3):180–189, 1969.
13. H. Fessler, C. C. Rogers, and P. Stanley. Stresses at keyway ends near shoulders. *Journal of Strain Analysis*, 4:267–277, 10 1969. ISSN 0022-4758. doi: 10.1243/03093247V044267. URL https://journals.sagepub.com/doi/10.1243/03093247V044267.
14. W. Orthwein. Power shafting: keys and keyways. Technical report, Paducah Gaseous Diffusion Plant, Ky.(USA), 1976.
15. W. C. Orthwein. Keyway stresses when torsional loading is applied by the keys: Stress concentrations are measured at keyway ends where helical fractures have begun in large-diameter shafts in torsion due to forces applied through the keys in these keyways. *Experimental Mechanics*, 15:245–248, 1975.
16. H. Ōkubo, K. Hosono, and K. Sakaki. The stress concentration in keyways when torque is transmitted through keys: The electroplating method of strain analysis is used to determine the peak stress at the corner of keyway. *Experimental Mechanics*, 8:375–380, 1968.
17. B. Hanel, E. Haibach, T. Seeger, G. Wirthgen, and H. Zenner. *FKM-Guideline Analytical strength assessment of components in mechanical engineering*. Forschungskuratorium Maschinenbau (FKM), Postfach 71 0864, D - 60498 Frankfurt / Main, 2003.
18. S. H. Loewenthal. New methodology for shaft design based on life expectancy. In *International Original Equipment Manufacturers Design Conference*, number E-3109, 1986.
19. S. H. Loewenthal. Factors that affect the fatigue strength of power transmission shafting and their impact on design. 1986.
20. D. Ntritsos, A. Tsolakis, and K. Giannakopoulos. Experimental and analytical approach of fatigue behavior of stepped ck45 shaft with adjacent key groove. *Procedia Structural Integrity*, 10:288–294, 2018.
21. W. D. Pilkey, D. F. Pilkey, and Z. Bi. *Peterson's stress concentration factors*. John Wiley & Sons, 2020.
22. M. Rossetto. *Introduzione alla fatica dei materiali e dei componenti meccanici*. Levrotto & Bella, Torino, 2000. ISBN 88-8218-061-1.
23. N. L. Pedersen. Optimization of keyway design. In *2nd International Conference on Engineering Optimization, Lisbon, Portugal*, 2010.
24. N. L. Pedersen. Stress concentrations in keyways and optimization of keyway design. *The journal of strain analysis for engineering design*, 45(8):593–604, 2010.
25. N. L. Pedersen. Optimal key design for shaft hub connections. *Proceedings of the Institution of Mechanical Engineers, Part C: Journal of Mechanical Engineering Science*, 238(3):811–821, 2024.
26. ASME. *Design of transmission shafting, ANSI/ASME B106.1M*. The American Society of Mechanical Engineers, New York, second printing edition, 1985.
27. J. E. Shigley. *Standard handbook of machine design.* McGraw Hill, New York, 3rd. edition, 2004. ISBN 0071441646.
28. H. J. Gough and H. Pollard. The strength of metals under combined alternating stresses. *Proceedings of the institution of mechanical engineers*, 131(1):3–103, 1935.
29. S. Loewenthal. Proposed design procedure for transmission shafting under fatigue loading. In *Ann. Meeting of the Natl. Conf. on Power Transmission*, number NASA-TM-78927, 1978.
30. M. Mascolo. Investigation of a broken crank mechanism: causes and possible solutions, 2023.
31. DIN 6885-UNI 6604-69. *UNI 6604-69 Linguette dimensioni e applicazione*. Ente di Unificazione Italiana, 1969.
32. Total materia. URL https://www.totalmateria.com/it.
33. Mindlin, Hucek, Harold and Gubiotti. *S*tructural alloys handbook, Mechanical Properties Data Center, 1982
34. F. M. Cura, G. Curti, et al. *Fondamenti di meccanica strutturale: Lezioni-Esercizi*. Clut, 2006.
35. Grote, K. & Hefazi, H. Springer *Handbook of mechanical engineering.* Springer Nature, 2021.
36. S. Venturini, C. Rosso, and M. Velardocchia. An automotive steel wheel digital twin for failure identification under accelerated fatigue tests. *Engineering Failure Analysis*, 2024.
37. J. Ding, W. Sum, R. Sabesan, S. Leen, I. McColl, and E. Williams. Fretting fatigue predictions in a complex coupling. *International Journal of Fatigue*, 2007.
38. W. S. Sum, E. J. Williams, and S. B. Leen. Finite element, critical-plane, fatigue life prediction of simple and complex contact configurations. *International Journal of Fatigue*, 2005.